Journal of Materials Chemistry A

COMMUNICATION

View Article Online
View Journal | View Issue

Cite this: J. Mater. Chem. A, 2016, 4, 3638

Received 21st December 2015
Accepted 18th January 2016

DOI: 10.1039/c5ta10467j

www.rsc.org/MaterialsA

High proton conductivity at low relative humidity in an anionic Fe-based metal–organic framework†

Thach N. Tu,[a] Nghi Q. Phan,[a] Thanh T. Vu,[a] Ha L. Nguyen,[a] Kyle E. Cordova*[ab] and Hiroyasu Furukawa*[abc]

A metal–organic framework, termed VNU-15 (VNU = Vietnam National University), was synthesized and subsequent detailed structural analysis revealed that the crystalline structure adopted the **fob** topology. Due to integrated sulphate ligands accompanied by hydrogen-bonded dimethylammonium ions that lined the pore channels of VNU-15, the proton conductivity of this material reached 2.90×10^{-2} S cm^{-1} at 95 °C and 60% relative humidity. Remarkably, the high proton conductivity of VNU-15 was maintained under these conditions, without any appreciable loss, for 40 h.

The development of novel electrolyte materials for proton exchange membrane fuel cells has received considerable attention owing to the need for alternative energy technologies.[1] Traditional electrolyte materials, such as fully hydrated Nafion, are capable of reaching proton conductivities of 1×10^{-1} S cm^{-1} at 80 °C.[2] However, to reach these levels, the material must remain in a relatively high humid environment (98% relative humidity, RH). This poses significant challenges, including substantial costs associated with maintaining the appropriate level of humidity as well as the possibility of flooding the cathode leading to a loss in fuel cell performance.[3] Furthermore, high operating temperatures, which lessen CO poisoning at Pt-based catalysts and increase efficiency, lead to decreased conductivities as a result of dehydration of the electrolyte material.[4] Therefore, the development of novel electrolyte materials that maintain high proton conductivity at elevated temperatures and under low relative humidity are highly sought after.[5]

Recently, metal–organic frameworks (MOFs) have been explored as potential candidates for use as electrolyte materials.[6] This is primarily due to the modular nature of MOF design and synthesis, in which the backbone components [*e.g.* inorganic and organic secondary building units (SBUs)] can be easily tailored to satisfy particular applications.[7] Indeed, previous work on developing MOFs as proton conducting materials have focused on incorporating proton transfer agents within the pores,[8–11] functionalizing coordinatively unsaturated metal sites,[12] tuning the acidity of the pore channels through incorporating specific functional groups,[13–17] and controlling and modifying defect sites,[18] among others.[19] These strategies have led to significant developmental progress, in which proton conductivities in MOFs have been achieved on the order of 10^{-2} S cm^{-1}, but require high working relative humidity (≥90% RH). On the other hand, proton conductivity under anhydrous conditions ($T \geq 100$ °C) in MOFs has reached high levels (10^{-2} S cm^{-1}), albeit in a limited number of reports.[8,20]

Herein, we report the synthesis and full characterization of a new iron-based anionic MOF, formulated as $Fe_4(BDC)_2(NDC)(SO_4)_4(DMA)_4$ (Fe(II)/Fe(III); BDC = benzene-1,4-dicarboxylate; NDC = naphthalene-2,6-dicarboxylate; DMA = dimethylammonium). Structural analysis revealed that this architecture, termed VNU-15 (where VNU = Vietnam National University), adopts the three-dimensional **fob** topology. Interestingly, VNU-15 was found to be composed of a new-type of infinite rod-shaped iron SBU, previously unseen in MOF chemistry. As a result of sulphate ligands coordinated to the iron SBUs, an ordered arrangement of DMA cations was found to line the pore channels of VNU-15 *via* hydrogen bonding leading to a plausible proton conduction pathway. Accordingly, proton conductivity measurements were undertaken, in which VNU-15 exhibited significant values at low RH and elevated temperatures (2.9×10^{-2} S cm^{-1} at 60% RH and 95 °C). Furthermore, time dependent measurements demonstrated that the performance of VNU-15 was maintained for at least 40 h

[a]Center for Molecular and NanoArchitecture (MANAR), Vietnam National University-Ho Chi Minh (VNU-HCM), Ho Chi Minh City 721337, Vietnam. E-mail: furukawa@berkeley.edu; kcordova@berkeley.edu

[b]Department of Chemistry, University of California-Berkeley, Materials Sciences Division, Lawrence Berkeley National Laboratory, Berkeley Global Science Institute, Berkeley, California 94720, USA

[c]Center of Research Excellence in Nanotechnology (CENT), King Fahd University of Petroleum and Minerals, Dhahran 31261, Saudi Arabia

† Electronic supplementary information (ESI) available: Full synthesis and characterization of VNU-15, crystallographic data, and additional proton conductivity measurement details. CCDC 1443413. For ESI and crystallographic data in CIF or other electronic format see DOI: 10.1039/c5ta10467j

at 60% RH and 95 °C without any appreciable loss in proton conductivity.

VNU-15 was prepared by dissolving $FeSO_4 \cdot 7H_2O$, 9,10-anthraquinone, $CuCl_2 \cdot 2H_2O$, H_2BDC and H_2NDC in *N*,*N*-dimethylformamide (DMF) in a borosilicate glass tube. The glass tube was then flamed sealed under ambient atmosphere and placed in an isothermal oven, pre-heated at 165 °C, for 72 h (Sections S1 and S2 in the ESI†). Reddish-yellow, octahedral-shaped single crystals were obtained in 71.3% yield based on iron. The roles of $CuCl_2 \cdot 2H_2O$ and 9,10-anthraquinone in the synthesis are presumed to be for catalysing the decarbonylation of DMF to form DMA and to serve as a redox agent, respectively. We note that VNU-15 could not be synthesized in the absence of either of these reagents even after exhaustive efforts were undertaken (Section S2†).

Single crystal X-ray diffraction (SCXRD) analysis revealed that VNU-15 crystallized in the orthorhombic space group, *Fddd* (No. 70), with unit cell parameters, $a = 16.7581$, $b = 18.8268$, and $c = 38.9998$ Å (Table S1†). The architecture of VNU-15 is based on two distinct linkers, namely BDC^{2-} and NDC^{2-}, that stitch together corrugated iron infinite rod SBUs. These infinite rod SBUs, formulated as $[Fe_2(CO_2)_3(SO_4)_2(DMA)_2]_\infty$, are composed of two independent octahedral iron atoms that alternate consecutively in order (Fig. 1a). The coordination environment of each distinct iron atom is highlighted by two equatorial corner-sharing vertices derived from μ_2-O atoms of the carboxylate functionality in NDC^{2-} (Fig. 1). It is noted that these μ_2-O atoms, which are *cis* to one another, are what promote the infinite rod SBU to arrange in a corrugated fashion. The coordination sphere of each iron is then completed through bridging axial sulphate ligands and bridging carboxylate functionalities from BDC^{2-} (Fig. 1b and c). Two BDC^{2-} and one NDC^{2-} linkers, relatively close together in space (aromatic π–π interaction distance, 3.4 Å), connect infinite rods together periodically in a perpendicular manner (83.4°) (Fig. 1d). This propagates a three-dimensional architecture with the **fob** topology (Fig. 1e). We deduce that the π–π interactions played an important role in forming the realized **fob** topological structure (Fig. 1d and e).[21] Finally, DMA counterions were found to line the infinite rod SBUs due to hydrogen bonding with the axial bridging sulphate ligands (N–H···O–S distances of 1.90–1.96 Å). Taken together, the resulting pore size of VNU-15, as calculated by PLATON,[22] is 2.52 Å.

The bulk phase purity of VNU-15 was confirmed by powder X-ray diffraction (PXRD) analysis, in which the as-synthesized diffraction pattern coincided with the pattern simulated from the single crystal structure (Fig. S2†). As-synthesized VNU-15 was then washed with copious amounts of DMF and dichloromethane to remove any unreacted starting materials before activation under reduced pressure at 100 °C for 12 h. Structural maintenance of VNU-15 after activation was proven by PXRD analysis (Fig. S2†). Elemental microanalysis (EA) was performed on VNU-15, in which the formulation determined by SCXRD was confirmed (calcd: C, 29.38; H, 4.62; N, 4.25; S, 8.29% and found: C, 28.95; H, 4.64; N, 4.74; S, 8.13%) (Section S2†). The absence of 9,10-anthraquinone is noted in both the SCXRD structural elucidation as well as in the EA data. To prove the absence of copper within the framework, atomic absorption spectroscopy was conducted on a digested, activated sample of VNU-15. Accordingly, a negligible amount of copper was found (Fe : Cu = 1 : 0.0022; 0.036 wt% of Cu), thus confirming that VNU-15 was entirely constructed from iron (Section S2†). Fourier transform infrared (FT-IR) spectroscopy analysis highlighted the presence of hydrogen-bonded DMA to sulphate ions that bridged two iron atoms in the activated sample of VNU-15. Specifically, a broad peak originating at 3400–3500 cm^{-1}, in conjugation with a sharp stretching peak at 2781 cm^{-1}, were assigned to N–H vibrations and C–H stretches of the DMA molecules, respectively (Fig. S3†). Furthermore, the vibration modes of the bridging sulphate ligands were clearly identified (sharp peaks, centred at 983, 1037, 1110, 1143 cm^{-1}) (Fig. S3†).

The framework thermal stability and architectural robustness of VNU-15 was assessed by thermal gravimetric analysis (TGA) and N_2 isotherms at 77 K. The TGA curve of VNU-15 exhibited a small weight percentage loss (<2 wt%) from room temperature to 200 °C. Furthermore, the residual metal oxide, attributed to Fe_3O_4, was in close agreement with that calculated from the crystal structure (24.3 and 23.4 wt% for the experimental and theoretical Fe_3O_4, respectively) (Fig. S4†). As

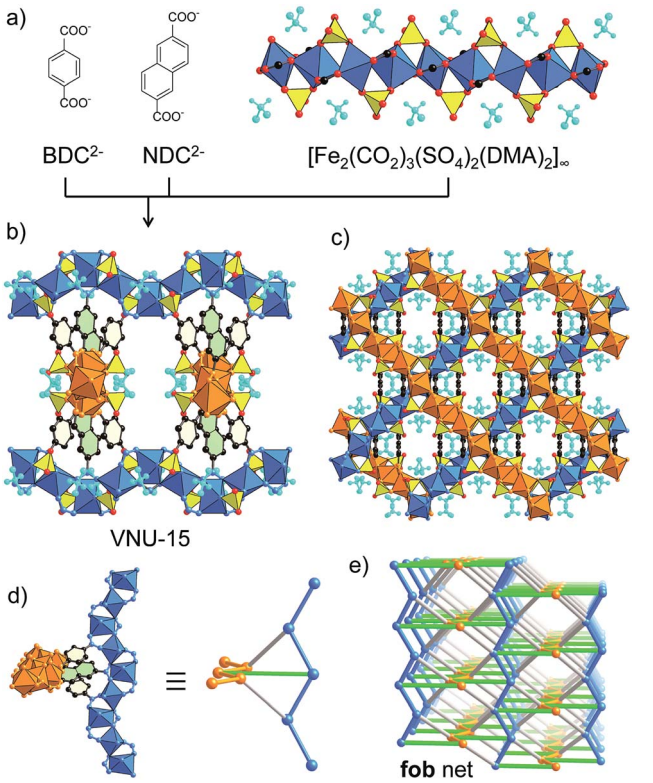

Fig. 1 Crystal structure of VNU-15 is constructed from BDC^{2-} and NDC^{2-} linkers that stitch together corrugated infinite rods of $[Fe_2(CO_2)_3(SO_4)_2(DMA)_2]_\infty$ (a). These corrugated infinite rods propagate along the *a* and *b* axes to form the three-dimensional architecture. The structure is shown from the [110] and [001] planes (b, c, respectively). Representation of the **fob** topology that VNU-15 adopts (d and e). Atom colours: Fe, orange and blue polyhedra; C, black; O, red; S, yellow; N, blue; and DMA cations, light blue. All other H atoms are omitted for clarity.

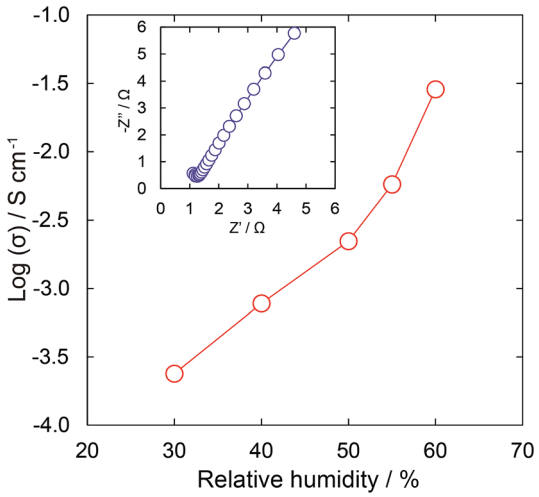

Fig. 2 Dependence of proton conductivity in VNU-15 as a function of relative humidity at 95 °C. Inset: Nyquist plot of VNU-15 at 60% RH and 95 °C.

expected, the N_2 isotherm at 77 K for VNU-15 displayed no appreciable uptake (Fig. S5†). This finding is due to the smaller pore size of VNU-15 with respect to the kinetic diameter of N_2. On the other hand, VNU-15 exhibited a high water uptake as demonstrated by the water sorption isotherm measured at 25 °C (102, 110 and 128 $cm^3\ g^{-1}$ at P/P_0 = 0.50, 0.55 and 0.60, respectively) (Fig. S6†).

Taking together the hydrogen-bonded DMA molecules lining the pore channels (plausible proton conduction pathway) as well as the high water uptake at low relative humidity, we sought to analyse the proton conductivity properties of this new architecture under practical conditions. Accordingly, we performed ac impedance measurements on a pelletized sample of VNU-15 from low relative humidity (30% RH) to medium humidity (60% RH) at an elevated temperature (95 °C) (Fig. 2 and Section S8†). The resulting Nyquist plots demonstrated the high conductivity of the VNU-15 pelletized sample with conductivity values increasing from 2.38×10^{-4} S cm^{-1} at 30% RH and 95 °C to 2.9×10^{-2} S cm^{-1} at 60% RH and 95 °C (Fig. 2). It is noted that the proton conductivity of VNU-15 at 60% RH and 95 °C is roughly 2.5 times higher than Nafion under similar conditions (1.0×10^{-2} S cm^{-1} at 60% RH and 80 °C) (Table 1). Additionally, we wish to point out that the high proton conductivity achieved by VNU-15 is on the order of a magnitude higher than that observed in several of the highest performing MOFs reported, albeit these materials' proton conductivity properties were reported with high working relative humidity (RH ≥ 90%) (Table 1).[23–25]

Table 1 Proton conductivity of VNU-15 in comparison with other water-mediated high proton conducting MOFs

Material	σ/S cm^{-1}	Conditions	Reference
Nafion	1.0×10^{-2}	60% RH, 80 °C	2
$\{[(Me_2NH_2)_3(SO_4)]_2[Zn_2(ox)_3]\}_n$	1.4×10^{-3}	60% RH, 25 °C	23
PCMOF-10	4.2×10^{-4}	70% RH, 70 °C	24
CPM-103a	8.0×10^{-3}	75% RH, 22.5 °C[a]	25
VNU-15	2.9×10^{-2}	60% RH, 95 °C	This work

[a] Performed using a single crystal; ox = oxalate.

To explore the proton-conduction mechanism, temperature-dependent proton conductivities of VNU-15 were measured at both 55% and 60% RH over a temperature range of 25–95 °C (Fig. 3). From the resulting Arrhenius plots, the activation energies were calculated to be 0.24 and 0.22 eV at 55% and 60% RH, respectively, indicating that the proton conduction of VNU-15 occurs through a Grotthuss mechanism (Fig. 3).[14] As shown in Fig. 3, the Arrhenius data was then cycled between the temperature ranges, which provided strong evidence for the stability of VNU-15 under these measurement conditions. The stability and structural maintenance of VNU-15 was further confirmed by PXRD analysis, in which a high degree of correspondence was observed between the simulated diffraction pattern and the diffraction pattern of a pelletized sample that was first exposed to 60% RH for 16 h and then used to perform ac impedance measurements (Section S9†). Additionally, FT-IR analysis supported the fact that the atomistic connectivity of VNU-15 was retained after exposing the sample to such conditions (Section S9†). Finally, in order to understand the working capacity of VNU-15 as a function of time, time-dependent ac impedance measurements were performed at 60% RH and 95 °C. Remarkably, it was found that VNU-15 maintained high proton conductivity (2.6×10^{-2} S cm^{-1}) for ≥40 h, without any observable loss in performance (Fig. 4).

In conclusion, we have succeeded in synthesizing an anionic iron-based MOF, termed VNU-15, that encompasses a new infinite rod SBU. The architecture of VNU-15 adopts the rare **fob** topology with pore channels that are densely occupied by a hydrogen-bonded network of sulphate ligands and DMA ions. As a result of this structural feature, VNU-15 was proven to exhibit high proton conductivity (2.9×10^{-2} S cm^{-1}) at the practical conditions of 60% RH and 95 °C. It is noted that the proton conductivity of VNU-15 is amongst the highest reported in MOF chemistry, especially when considering practical operating conditions.

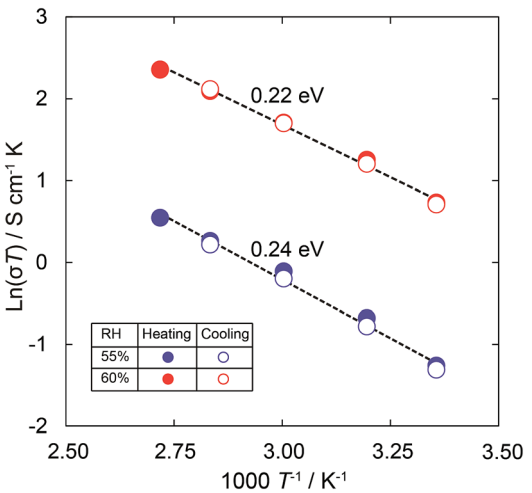

Fig. 3 Arrhenius plot of VNU-15 depicting the heating (closed circles) and cooling (open circles) cycles at 60% RH (red) and 55% RH (blue).

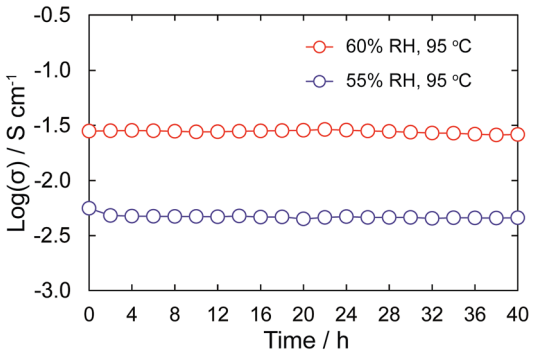

Fig. 4 Time-dependent proton conductivity of VNU-15 at 55% RH (blue circles) and 60% RH (red circles) and 95 °C.

Acknowledgements

This work was financially supported by VNU-HCM (A2015-50-01-HĐ-KHCN) and the United States Office of Naval Research Global: Naval International Cooperative Opportunities in Science and Technology Program (No. N62909-15-1N056). We are grateful to Prof. O. M. Yaghi (UC Berkeley) for his continued support of MANAR. We acknowledge Mr T. L. H. Doan and Mr N. T. Hoang at MANAR for their valuable discussion and assistance on this work. We are grateful to Prof. D. Prosperio (University of Milan) for his assistance on the topological analysis of VNU-15. We thank Mr J. Yang (UC Berkeley) for performing the elemental microanalysis measurements. Finally, we appreciate the inputs provided by Profs. P. T. S. Nam (University of Technology, VNU-HCM) and H. T. Nguyen (University of Science, VNU-HCM).

References

1 B. C. H. Steele and A. Heinzel, *Nature*, 2001, **414**, 345–352; Y. J. Wang, N. Zhao, B. Fang, H. Li, X. T. Bi and H. Wang, *Chem. Rev.*, 2015, **115**, 3433–3467.
2 Z. Li, G. He, B. Zhang, Y. Cao, H. Wu, Z. Jiang and Z. Tiantian, *ACS Appl. Mater. Interfaces*, 2014, **6**, 9799–9807; Y. Sone, P. Ekdunge and D. Simonsson, *J. Electrochem. Soc.*, 1996, **143**, 1254–1259.
3 Q. Li, R. He, J. O. Jensen and N. J. Bjerrum, *Chem. Mater.*, 2003, **15**, 4896–4915; Y. Chen, M. Thorn, S. Christensen, C. Versek, A. Poe, R. C. Hayward, M. T. Tuominen and S. Thayumanavan, *Nat. Chem.*, 2010, **2**, 503–508.
4 G. Kim and S. H. Jhi, *ACS Nano*, 2011, **5**, 805–810.
5 K. E. Martin and J. P. Kopasz, *Fuel Cells*, 2009, **9**, 356–362.
6 M. Yoon, K. Suh, S. Natarajan and K. Kim, *Angew. Chem., Int. Ed.*, 2013, **52**, 2688–2700.
7 H. Furukawa, K. E. Cordova, M. O'Keeffe and O. M. Yaghi, *Science*, 2013, **341**, 1230444.
8 V. G. Ponomareva, K. A. Kovalenko, A. P. Chupakhin, D. N. Dybtsev, E. S. Shutova and V. P. Fedin, *J. Am. Chem. Soc.*, 2012, **134**, 15640–15643.
9 D. N. Dybtsev, V. G. Ponomareva, S. B. Aliev, A. P. Chupakhin, M. R. Gallyamov, N. K. Moroz, B. A. Kolesov, K. A. Kovalenko, E. S. Shutova and V. P. Fedin, *ACS Appl. Mater. Interfaces*, 2014, **6**, 5161–5167.
10 M. Bazaga-Garcia, R. M. Colodrero, M. Papadaki, P. Garczarek, J. Zon, P. Olivera-Pastor, E. R. Losilla, L. Leon-Reina, M. A. Aranda, D. Choquesillo-Lazarte, K. D. Demadis and A. Cabeza, *J. Am. Chem. Soc.*, 2014, **136**, 5731–5739.
11 W. J. Phang, W. R. Lee, K. Yoo, D. W. Ryu, B. Kim and C. S. Hong, *Angew. Chem., Int. Ed.*, 2014, **53**, 8383–8387.
12 N. C. Jeong, B. Samanta, C. Y. Lee, O. K. Farha and J. T. Hupp, *J. Am. Chem. Soc.*, 2012, **134**, 51–54; G. Xu, K. Otsubo, T. Yamada, S. Sakaida and H. Kitagawa, *J. Am. Chem. Soc.*, 2013, **135**, 7438–7441.
13 S. Kim, K. W. Dawson, B. S. Gelfand, J. M. Taylor and G. K. H. Shimizu, *J. Am. Chem. Soc.*, 2013, **135**, 963–966.
14 A. Shigematsu, T. Yamada and H. Kitagawa, *J. Am. Chem. Soc.*, 2011, **133**, 2034–2036.
15 S. Sen, N. N. Nair, T. Yamada, H. Kitagawa and P. K. Bharadwaj, *J. Am. Chem. Soc.*, 2012, **134**, 19432–19437; X. Y. Dong, R. Wang, J. Z. Wang, S. Q. Zang and T. C. W. Makac, *J. Mater. Chem. A*, 2015, **3**, 641–647.
16 J. M. Taylor, K. W. Dawson and G. K. H. Shimizu, *J. Am. Chem. Soc.*, 2013, **135**, 1193–1196.
17 W. J. Phang, H. Jo, W. R. Lee, J. H. Song, K. Yoo, B. Kim and C. S. Hong, *Angew. Chem., Int. Ed.*, 2015, **54**, 5142–5146.
18 J. M. Taylor, S. Dekura, R. Ikeda and H. Kitagawa, *Chem. Mater.*, 2015, **27**, 2286–2289.
19 P. Ramaswamy, N. E. Wong and G. K. Shimizu, *Chem. Soc. Rev.*, 2014, **43**, 5913–5932; N. T. T. Nguyen, H. Furukawa, F. Gándara, C. A. Trickett, H. M. Jeong, K. E. Cordova and O. M. Yaghi, *J. Am. Chem. Soc.*, 2015, **137**, 15394–15397; D. Umeyama, S. Horike, M. Inukai and S. Kitagawa, *J. Am. Chem. Soc.*, 2013, **135**, 11345–11350; D. Umeyama, S. Horike, M. Inukai, T. Itakura and S. Kitagawa, *J. Am. Chem. Soc.*, 2012, **134**, 12780–12785; S. Horike, D. Umeyama, M. Inukai, T. Itakura and S. Kitagawa, *J. Am. Chem. Soc.*, 2012, **134**, 7612–7615; D. Umeyama, S. Horike, M. Inukai, Y. Hijikata and S. Kitagawa, *Angew. Chem., Int. Ed.*, 2011, **50**, 11706–11709; J. A. Hurd, R. Vaidhyanathan, V. Thangadurai, C. I. Ratcliffe, I. L. Moudrakovski and G. K. H. Shimizu, *Nat. Chem.*, 2009, **1**, 705–710.
20 V. G. Ponomareva, K. A. Kovalenko, A. P. Chupakhin, E. S. Shutova and V. P. Fedin, *Solid State Ionics*, 2012, **225**, 420–423; S. Horike, W. Chen, T. Itakura, M. Inukai, D. Umeyama, H. Asakurae and S. Kitagawa, *Chem. Commun.*, 2014, **50**, 10241–10243.
21 M. O'Keeffe, M. A. Peskov, S. J. Ramsden and O. M. Yaghi, *Acc. Chem. Res.*, 2008, **41**, 1782–1789.
22 A. L. Spek, *Acta Crystallogr., Sect. D: Biol. Crystallogr.*, 2009, **65**, 148–155.
23 S. S. Nagarkar, S. M. Unni, A. Sharma, S. Kurungot and S. K. Ghosh, *Angew. Chem., Int. Ed.*, 2014, **126**, 2676–2680.
24 P. Ramaswamy, N. E. Wong, B. S. Gelfand and G. K. H. Shimizu, *J. Am. Chem. Soc.*, 2015, **137**, 7640–7643.
25 Q. G. Zhai, C. Mao, X. Zhao, Q. Lin, F. Bu, X. Chen, X. Bu and P. Feng, *Angew. Chem., Int. Ed.*, 2015, **54**, 7886–7890.